Journal of Power Sources 662 (2026) 238753

Contents lists available at ScienceDirect

Journal of Power Sources

journal homepage: www.elsevier.com/locate/jpowsour

Ethylene sulfate-enabled stable interphases in fluorinated ether electrolytes for high-performance sodium-ion batteries

Rishivandhiga Jayakumar [a,b,1], Chanmonirath Michael Chak [a,b,c,1], Vadim Shipitsyn [a,b,c,1], Yuwei Zhu [d], Yunyuan Lu [d], Glenn Pastel [e,*], Zhiao Yu [f,**], Linqin Mu [d,***], Wenhua Zuo [g], Lin Ma [a,b,c,****]

[a] Department of Mechanical Engineering and Engineering Science, The University of North Carolina at Charlotte, Charlotte, NC, 28223, USA
[b] Battery Complexity, Autonomous Vehicle and Electrification (BATT CAVE) Research Center, The University of North Carolina at Charlotte, Charlotte, NC, 28223, USA
[c] Department of Applied Physical Sciences, The University of North Carolina at Chapel Hill, Chapel Hill, NC, 27514, USA
[d] Materials Science Engineering, School of Engineering for Matter, Transport, and Energy, Arizona State University, Tempe, AZ, 85281, USA
[e] Battery Sciences Branch, DEVCOM Army Research Laboratory, Adelphi, MD, 20783, USA
[f] Feon Energy Inc., Woburn, MA, 01801, USA
[g] Chemical Sciences and Engineering Division, Argonne National Laboratory, Lemont, IL, 60439, USA

HIGHLIGHTS

- DTD in F4DEE forms NaF- and S-rich SEI, improving anode stability.
- DTD-F4DEE CEI suppresses electrolyte oxidation at high voltage.
- 500 cycles at C/5: ~88 % retention (25 °C) and ~82 % (40 °C) with negligible gas.
- DTD-F4DEE mitigates cathode–anode cross-talk, reducing impedance and gas.

ARTICLE INFO

Keywords:
Non-aqueous sodium-ion batteries
Fluorinated ether solvent
Ethylene sulfate additive
Cross-talk

ABSTRACT

Sodium-ion batteries (SIBs) with earth-abundant materials are promising for grid-scale energy storage, but in carbonate electrolytes, parasitic electrode-electrolyte reactions cause excessive capacity fade and impedance growth. This study focuses on interphase engineering via ethylene sulfate (DTD) additive in 1,2-bis(2,2-difluoroethoxy)ethane (F4DEE)-based electrolytes for $Na_{0.97}Ca_{0.03}[Mn_{0.39}Fe_{0.31}Ni_{0.22}Zn_{0.08}]O_2$ (NCMFNZO)/hard carbon (HC) pouch cells up to 4.0 V. During formation, the DTD-containing electrolyte forms a NaF and sulfur-rich solid electrolyte interphase (SEI) on the HC anode, as confirmed by X-ray photoelectron spectroscopy (XPS), and a robust cathode electrolyte interphase (CEI) that suppresses electrolyte oxidation, as evidenced by soft X-ray absorption spectroscopy (XAS). Impressive reversibility is observed after cycling for 500 cycles at C/5 with ~88 % capacity retention at 25 °C and ~82 % at 40 °C and negligible gas evolution. Pouch bag configurations with isolated electrodes reveal that DTD mitigates cathode-anode cross-talk during 500 h storage at 40 °C, thereby reducing impedance growth and gas production. Soft XAS further verifies the CEI's oxidation-suppressing function with or without cross-talk. These interphase insights highlight how DTD-F4DEE synergize for high-voltage SIB longevity, and should serve as a good test platform for future studies addressing Na plating failure mechanisms.

* Corresponding authors.
** Corresponding author.
*** Corresponding authors.
**** Corresponding author. Department of Applied Physical Sciences, The University of North Carolina at Chapel Hill, Chapel Hill, NC, 27514, USA.
E-mail addresses: glenn.r.pastel.civ@army.mil (G. Pastel), zhiao.yu@feonenergy.com (Z. Yu), linqinmu@asu.edu (L. Mu), l.ma@unc.edu (L. Ma).
[1] these authors contributed equally.

https://doi.org/10.1016/j.jpowsour.2025.238753
Received 25 August 2025; Received in revised form 21 October 2025; Accepted 31 October 2025

1. Introduction

The widespread adoption of lithium-ion batteries (LIBs) has accelerated global electrification and decarbonization efforts, particularly in electric vehicles and grid energy storage [1]. However, escalating energy demands necessitate complementary electrochemical storage technologies to alleviate reliance on LIBs [2]. Sodium-ion batteries (SIBs) have emerged as one of the most promising alternatives for grid-scale applications, owing to their utilization of earth-abundant elements such as sodium (Na), manganese (Mn), iron (Fe), and carbon (C) [3,4]. Despite these advantages, achieving exceptionally long lifetimes in SIBs remains challenging, primarily due to parasitic reactions between electrodes and electrolytes, which lead to capacity fade, and impedance growth.

Rational electrolyte design represents an efficient strategy to mitigate these issues by engineering stable electrode–electrolyte interphases (EEI) [5,6]. This approach has yielded initial successes in SIBs across various electrolyte components. From a salt perspective, replacing sodium hexafluorophosphate ($NaPF_6$) with sodium bis(fluorosulfonyl) imide (NaFSI) has been shown to reduce electrolyte decomposition products and tape degradation, correlating with improved cycling performance [7,8]. In terms of solvents, substituting dimethyl carbonate (DMC) with diethyl carbonate (DEC) similarly minimizes decomposition and enhances stability [7]. Additionally, Jin et al. [9] demonstrated that a DMC/tris (2,2,2-trifluoroethyl) phosphate (TFP) solvent mixture enables stable cycling (90 % capacity retention after 300 cycles) in $NaNi_{0.68}Mn_{0.22}Co_{0.1}O_2$/hard carbon (HC) cells at 4.2 V. Regarding electrolyte additives, Hijazi et al. [10,11] reported that prop-1-ene-1, 3-sultone (PES), sodium difluorophosphate, and ethylene sulfate (DTD) effectively reduce gas generation and parasitic reaction heat flow in $Na_{0.97}Ca_{0.03}[Mn_{0.39}Fe_{0.31}Ni_{0.22}Zn_{0.08}]O_2$ (NCMFNZO)/HC pouch cells, thereby extending lifetime. Notably, DTD suppresses cathode-anode cross-talk, a common cell failure mechanism [12,13], achieving >90 % capacity retention after 13 months of cycling at 40 °C up to 3.8 V in carbonate-based electrolytes [10].

However, most electrolyte optimization efforts have focused on carbonate-based solvents, which suffer from limited anodic stability at high voltages (>3.8 V) [11], impeding further improvements in energy density and lifetime for SIBs. Recent advancements in fluorinated ether solvents [14–16], such as 1,2-bis(2,2-difluoroethoxy)ethane (F4DEE) [15], offer promising solutions for high-voltage operation due to their enhanced oxidative stability. However, their application has been largely confined to lithium-based systems, leaving uncertainties regarding performance in SIBs and compatibility with proven additives like DTD. Addressing this gap is important to unlocking the full potential of fluorinated ethers for high-voltage, long-lifetime SIBs in grid storage.

In this work, we investigate the synergistic effects of DTD additive in a fluorinated ether (i.e. F4DEE)-based electrolyte on the performance of NCMFNZO/HC sodium-ion pouch cells. Through electrochemical testing, gas analysis, and advanced interphasial characterizations including X-ray photoelectron spectroscopy (XPS) and soft X-ray absorption spectroscopy (XAS), we demonstrate enhanced interphase stability, reduced parasitic reactions, and extended cycling lifetime up to 4.0 V at both 25°C and 40°C. Specifically, the DTD-containing electrolyte forms a robust cathode electrolyte interphase (CEI) that suppresses electrolyte oxidation at the cathode during formation, while mitigating cathode-anode cross-talk during CEI evolution. These results highlight the potential of fluorinated ether electrolytes paired with suitable electrolyte additives for high-voltage, long-lifetime SIBs in grid storage applications.

2. Materials and methods

2.1. Electrode and electrolyte preparation

NCMFNZO/HC dry pouch cells (210 mAh capacity, Lifun Technology, Zhuzhou, Hunan) were obtained, with details reported previously [13,17]. The cathode and anode active materials are loaded at 16 mg cm^{-2} and 9.47 mg cm^{-2}, respectively, using aluminum foil current collectors with an active electrode area of ~99.58 cm^2. For symmetric cell fabrication, pouch cells were disassembled in a glovebox, and the jelly roll was unrolled to separate the cathode and anode. Single-side-coated cathodes were prepared by removing electrode material from one side of the current collector using N-methyl pyrrolidone (NMP). Cathode and anode samples (0.95 cm^2) were punched for coin cells. Symmetric 2032-coin cells were assembled with a polypropylene blown microfiber (BMF) separator and ~150 μL of electrolyte. Electrolytes were prepared using molality, with 1m NaFSI (purity >99.0 %, Zhuhai Smoothway Electronic Materials Co. Ltd.) in F4DEE (purity >99.5 %, H_2O < 20 ppm, Feon Energy Inc.) as the control. Additive-containing electrolytes were formulated by dissolving DTD (H_2O < 20 ppm, Capchem) into the control electrolyte at 2 wt% ratio.

2.2. Electrochemical measurements

Electrochemical measurements were conducted on NCMFNZO/HC dry pouch cells filled with 1 g of electrolyte and sealed using a compact vacuum sealer (MSK-115A-111, MTI Corp.) at −85 kPa gauge pressure, 165 °C, and 5 s in an Ar-filled glovebox. During formation, cells were placed in temperature-controlled chambers at 40 ± 0.1 °C (Neware Battery Testing System, Shenzhen), rested for 3 h, charged to 4 V at C/20, and discharged to 3.1 V at C/20 for degassing. Long-term cycling tests were performed between 1.5 V and 4.0 V at 25 °C and 40 °C using constant current constant voltage (CCCV) mode at C/5 with a C/20 cut-off current, with a check-up cycle every 50 cycles at C/20 to evaluate capacity loss due to Na inventory loss. For storage testing, cells underwent two cycles (discharge to 1.5 V, charge to 4.0 V at C/20, 40 °C), followed by 500-h storage at open circuit voltage. Desodiated NCMFNZO and sodiated HC electrodes, collected at 4.0 V from full cells, were sealed in separate pouch bags (same material as pouch cells) with 0.5 g of control electrolyte and stored for 500 h at 40°C[13]. Electrochemical impedance spectroscopy (EIS) was performed using a Biologic VMP3, collecting ten data points per decade from 100 kHz to 100 mHz with a 10 mV signal amplitude at 25 °C.

2.3. Cells and materials characterization

Gas generated in NCMFNZO/HC pouch cells or pouch bags during formation, storage, and cycling was quantified using Archimedes' principle, as described by Aiken et al. [18]. Electrodes were extracted from pouch cells in an argon-filled glovebox, rinsed with anhydrous DMC, dried under vacuum in an antechamber overnight, and transferred to an XPS system via a sealed vacuum setup. XPS data were collected using a survey scan (pass energy 224 eV, step size 0.4 eV) and high-resolution scan (pass energy 55 eV, step size 0.05 eV), with surface neutralization achieved via low-energy Ar-ion flow and an electron neutralizer. The X-ray (25 W) was focused to a 100 μm spot. XPS spectra were fitted with 70/30 Gaussian/Lorentzian line shapes on a Shirley background using PHI Multipak software (v. 9.6), with peaks adjusted to the C1s sp3 binding energy (284.8 eV) to correct for surface charging. Soft XAS measurements were conducted at the Stanford Synchrotron Radiation Light source (SSRL) on beamline 8-2 at a 55° incidence angle (magic angle) of X-ray incidence. The spectra were recorded using the 1000 lines/mm grating operated with 60*60 μm slits for the Ni L-edge data (~0.35 eV resolution). The spot size at the interaction point was around 1 × 1 mm^2 and the total flux was in the order of 10^{10} photons/s for which beam damage was not noticeable even for extended exposure. The data were collected both in the total electron yield (TEY) and total fluorescence yield (TFY) modes using the drain current (amplified by a Keithley picoammeter) for TEY and a Silicon Diode (IRD AXUV-1000) for TFY. The incoming flux was recorded using a nickel grid with an Au sputtered film (i0), collected in TEY, mounted upstream of the end

station. Powder or electrode samples were loaded on carbon tape and then stuck to an aluminum sample holder. XAS samples were mounted on an aluminum holder with double-sided carbon tape in an Ar-filled glovebox and transferred to the load-lock chamber in a double-contained, argon-purged glove bag. Data were normalized using PyMCA software.

3. Results and discussion

Using NCMFNZO/HC pouch cells, the impact of F4DEE-based electrolytes on cell formation was evaluated. A 1m NaFSI in F4DEE electrolyte served as the control and was selected instead of a $NaPF_6$ composition due to its superior stability against HF formation from reactions with trace water [7]. Following previous report [10,11], an optimized concentration of 2 wt% DTD additive was chosen for its demonstrated enhancement in SIB performance. During formation, both control and DTD-containing electrolytes yielded a successful first-cycle charge and discharge process (Fig. S1), indicating effective passivation of the HC anode. Gas generation during the initial charge to 4.0 V, quantified via Archimedes' principle, was minimal (<0.1 mL) for both electrolyte formulations (Fig. S1).

The effect of electrolyte composition on electrochemical behavior and interphase chemistry during formation was then investigated. Electrochemical impedance spectroscopy (EIS) of the pouch cells at 25 °C was used to assess charge transfer resistance (R_{ct}, Fig. 1a–c), which indicates the resistance to electrochemical reactions at the electrode–electrolyte interface. This resistance reflects the process where Na^+ or Na either gain or lose electrons to form neutral Na or revert to Na^+, facilitating their incorporation into or departure from the electrode material. Each spectrum, averaged from two tests, was fitted using an equivalent circuit (Fig. S2) to determine R_{ct}. Contact resistance values of 8 Ω cm^2 for the NCMFNZO cathode and 6 Ω cm^2 for the HC anode, derived from prior studies [13] using blocking electrodes at 0 % state of charge (SOC) to prevent Na^+ intercalation and faradaic reactions, were applied for fitting. Based on the Nyquist plot (Fig. 1a) and equivalent circuit fitting (Supplementary Table 1**), the R_{ct} of cells with 2 wt% DTD additive is slightly higher than that of cells with the control electrolyte (i.e. 1m NaFSI in F4DEE) after formation. To identify whether the R_{ct} increase originates primarily from the cathode or anode, EIS with equivalent circuit fitting was conducted on symmetric cells** (Fig. 1b–c, Supplementary Table 1). The results show that adding 2 wt% DTD primarily increases R_{ct} at the NCMFNZO cathode side, while the HC anode exhibits nearly identical R_{ct} to the control.

To confirm the formation of solid electrolyte interphase (SEI) on the HC anode in NCMFNZO/HC pouch cells with both control and DTD-containing electrolytes, XPS analysis was performed (Fig. 1d–f). Unlike fresh HC anodes, which show no F 1s signal per prior studies [13], the control electrolyte induces NaF formation on the HC anode (Fig. 1d), consistent with the reduction of the fluorinated ether, as reported previously [19]. Adding 2 wt% DTD also results in the presence of NaF (Fig. 1e) and the S 2p spectra (Fig. 1f) confirms DTD reduction by peaks

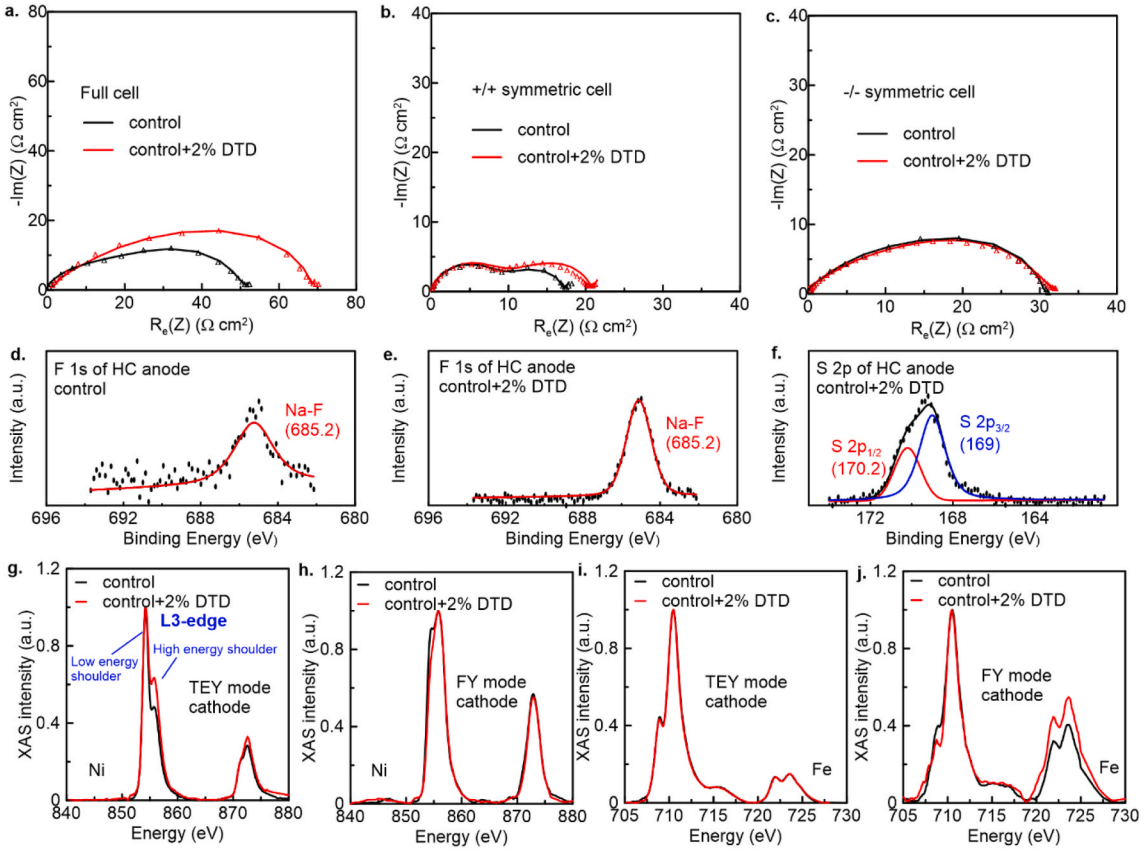

Fig. 1. Evaluation of the effects of electrolyte composition on the formation process of NCMFNZO/HC pouch cells. (a) Nyquist plot of the area specific impedance of NCMFNZO/HC pouch cells at 3.1 V after cell formation. 3.1 V corresponds to roughly 50 % state of charge, a relatively stable condition suitable for comparison with previously reported Nyquist plots. Nyquist plot of the area specific impedance of (b) NCMFNZO/NCMFNZO symmetric cells ((+/+)/2) and (c) HC/HC symmetric cells ((−/−)/2) reconstructed from NCMFNZO/HC pouch cells at 3.1 V after formation. All impedance measurements were performed at 25 °C. Experimental data are shown as solid line and fitted data are shown as triangle symbol. Each spectrum is the average results of two cells measurement. (d) XPS spectra of F 1s for HC anode with control electrolyte corresponding to (c). (e) XPS spectra of F 1s for HC anode with the electrolyte of control+2 % DTD corresponding to (c). (f) XPS spectra of S 2p for HC anode with the electrolyte of control+2 % DTD corresponding to (c). Soft XAS spectroscopy of Ni L-edge in (g) TEY and (h) FY mode for NCMFNZO cathode corresponding to (b). Soft XAS spectroscopy of Fe L-edge in (i) TEY and (j) FY mode for NCMFNZO cathode corresponding to (b).

at 168.5–169.5 eV attributable to sulfate (e.g., Na_2SO_4) and sulfite (e.g., $ROSO_2Na$) species [20]. N 1s spectra (Fig. S3) were collected to understand FSI^- involvement in SEI formation. The presence of nitrogen indicates FSI^- decomposition as DTD contains no N. N–S features appear in both samples [21] but with higher signal-to-noise in the control + 2 % DTD sample, suggesting FSI^- decomposition could occur in the control and be promoted by DTD. Because FSI^- and DTD reduction pathways and potentials could be strongly influenced by the electrolyte solvation structure, detailed mechanistic insight will require targeted solvation studies and complementary theoretical calculations in future work.

Given that the observed R_{ct} increase is primarily from the NCMFNZO cathode side after formation, the CEI was investigated using both XPS and ensemble-averaged and surface-sensitive soft XAS. XPS (F 1s, Fig. S4) shows C–F and Na–F signals in the control electrolyte, which could arise from CEI contributions of F4DEE or FSI^-. With 2 % DTD the Na–F peak is absent and the C–F signal is weak (i.e. low signal-to-noise), consistent with binder-derived C–F as reported previously [13]. These data indicate that DTD decomposition products could dominate or mask the CEI signature on the cathode surface. During soft XAS characterization, fluorescence yield (FY) and total electron yield (TEY) modes were used to probe subsurface (50 nm) and surface (10 nm) chemical environments, respectively. Transition metal oxidation states were monitored by the intensity ratio of the high-to low-energy shoulders in the L3-edge spectra, with a higher ratio indicating increased oxidation states [22,23]. Comparing FY and TEY spectra revealed depth-dependent chemical changes influenced by electrolyte composition during formation. The DTD-containing electrolyte showed a higher average Ni oxidation state in both TEY and FY modes (Fig. 1g–h). These results show that Ni reduction occurs at the surface of the control sample despite electrochemical oxidation of Ni in the bulk, driven by electrolyte oxidation. In contrast, the CEI formed with 2 wt% DTD additive exhibits improved stability, effectively suppressing electrolyte oxidation and mitigating Ni reduction at the surface. TEY results showed no significant Fe oxidation state difference between electrolytes (Fig. 1i), but FY data revealed a slightly higher average Fe oxidation state with the addition of DTD (Fig. 1j), further supporting improved CEI stability against electrolyte oxidation during formation. Mn oxidation states remained consistent at Mn^{4+} on the surface across both samples (Fig. S5).

To study the effect of electrolyte composition on the cycling lifespan of SIBs, NCMFNZO/HC pouch cells were cycled at a C/5 rate in CCCV mode with a C/20 cut-off current, between 1.5 V and 4.0 V, at 25 °C and 40 °C, with periodic C/20 check-up cycles every 50 cycles to evaluate Na inventory loss. In addition to the ether-based control electrolyte and control +2 % DTD, a conventional carbonate electrolyte was also tested: 1 m NaFSI in ethylene carbonate (EC)/DMC (15/85 by weight) + 2 % DTD, because DTD is particularly effective in carbonate systems at extending SIB lifetime and mitigating cathode–anode cross-talk [10]. Control +2 wt% DTD electrolyte improves capacity retention in NCMFNZO/HC pouch cells compared to both control cells and carbonate electrolyte containing cells at both 25 °C and 40 °C, particularly in mitigating Na inventory loss, as evidenced by C/20 check-up cycle results (Fig. 2). Specifically, control +2 wt% DTD-containing cells achieve ~88 % capacity retention after 500 cycles at 25 °C (Fig. 2a–d) and ~82 % retention at 40 °C (Fig. 2e–h), with negligible gas generation (Fig. S6). Notably, control cells exhibit the worst cycling performance with larger amounts of gas generation at 25 °C than at 40 °C (Fig. S6), a counter-intuitive trend likely due to higher polarization growth at the lower temperature (Fig. 2c and g). Future studies should explore F4DEE-derived interphase properties as a function of temperature, though this is beyond the scope of the present study. F4DEE replacing traditional carbonates extends cell lifetime (Fig. 2) at both 25 °C and 40 °C up to 4.0 V when the same 2 wt% DTD additive is used, demonstrating this solvent's advantage in SIBs. This improvement could be due to (1) the well-known strong anti-oxidation capability of F4DEE [14,15] and (2) a potential interphase synergy between F4DEE and DTD, since F4DEE has been identified here to contribute to interphase formation. All cells show Na plating on the HC anode after cycling (Fig. S7), regardless of DTD. This indicates the SEI formed with DTD did not reduce the overpotential enough to prevent Na plating. Na plating contributes to capacity fade by consuming cyclable Na and promoting severe side reactions with the electrolyte. Its tendency to form clusters or dendrites also introduces safety risks from internal short circuits. In this study we cannot determine exactly when plating occurs or quantify its contribution to capacity loss. These aspects warrant further

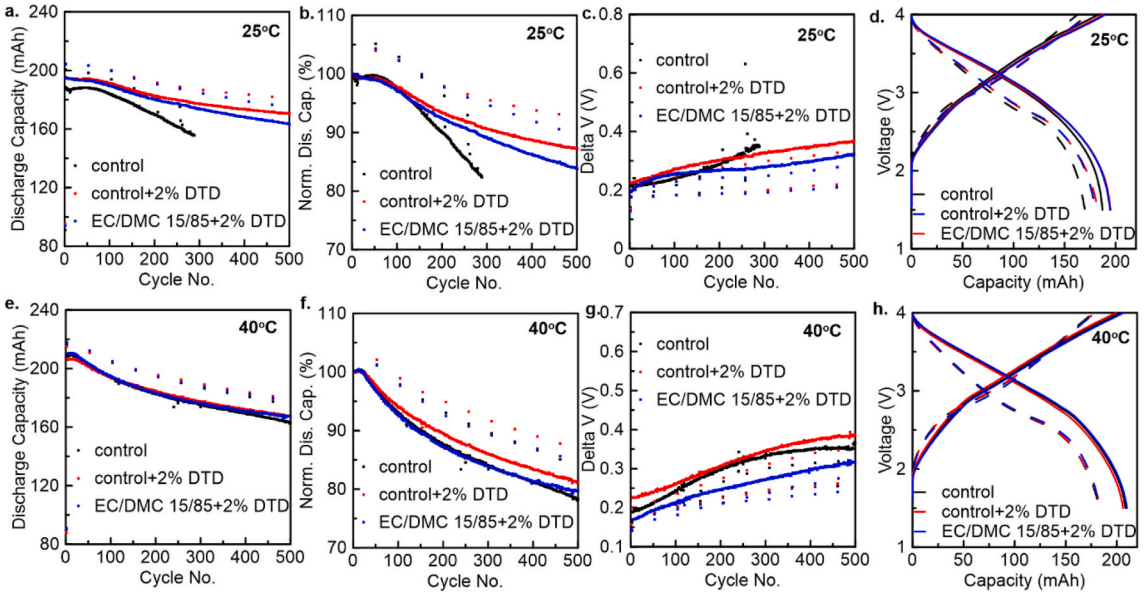

Fig. 2. Electrochemical performance of NCMFNZO/HC pouch cells with three electrolytes: 1 m NaFSI in F4DEE (control), control + 2 % DTD, and 1 m NaFSI in EC/DMC (15/85) + 2 % DTD. (a) Discharge capacity, (b) normalized discharge capacity, (c) delta V vs. cycling No. (note: delta V is the difference between average charge voltage and average discharge voltage), and (d) corresponding voltage vs. capacity during long-term cycling between 1.5 and 4.0 V at 25 °C with a rate of C/5 in CCCV mode with a C/20 cut-off current. Solid line: cycle 5; dashed line: cycle 200. (e) Discharge capacity, (f) normalized discharge capacity, (g) delta V vs. cycling No., and (h) corresponding voltage vs. capacity during long-term cycling between 1.5 and 4.0V at 40 °C with a rate of C/5 in CCCV mode with a C/20 cut-off current. C/20 was performed every 50 cycles. Solid line: cycle 5; dashed line: cycle 200.

investigation in future work.

Cross-talk is an important cell failure pathway. To assess how electrolyte composition with F4DEE solvent affects cathode–anode cross-talk, we investigated impedance and gas evolution (Fig. 3). Specifically, we isolated cathode-anode cross-talk by disassembling pouch cells after formation with separated cathodes and anodes at 4.0 V (Fig. 3a) and subjected them to storage at 40 °C for 500 h. For comparison, pouch cells with intact cathode-anode cross-talk were stored under identical conditions (40 °C, 500 h). Regarding gas evolution (Fig. 3b), the HC anode side showed minimal gas generation during storage for both the control electrolyte and the 2 wt% DTD-containing electrolyte. In contrast, on the NCMFNZO cathode side, the control electrolyte produced significantly more gas than the 2 wt% DTD-containing electrolyte. This suggests that the CEI formed with DTD effectively suppresses side reactions between the desodiated NCMFNZO cathode and the F4DEE-based electrolyte, reducing gas generation. Comparing gas production from isolated NCMFNZO cathodes (no cathode-anode cross-talk) to pouch cells with intact cathode-anode cross-talk, the former generated more gas, indicating that some gas is consumed by the anode through cathode-anode cross-talk. To investigate the impact of cathode-anode cross-talk on R_{ct}, symmetric cells were constructed, and EIS was performed at 25 °C (Fig. 3c–d) and 10 °C (Fig. 3e–f, Supplementary Table 2). When F4DEE was used as the solvent, the control electrolyte without DTD exhibited a significant R_{ct} increase at the NCMFNZO cathode in the absence of cathode-anode cross-talk. However, this R_{ct} increase was substantially mitigated with the addition of 2 wt% DTD, highlighting its role in mitigating cross-talk (Fig. 3c–e). On the HC anode side, cathode-anode cross-talk had a negligible effect on R_{ct}, regardless of DTD addition (Fig. 3d–f).

To elucidate the role of DTD in suppressing impedance increase of the NCMFNZO cathode under conditions free of cross-talk, we examined the CEI evolution post-storage, both in the presence and absence of cross-talk, via soft XAS employing TEY and FY detection. These modes enable probing of top-surface layers (10 nm depth) and subsurface regions (50 nm depth), respectively (Fig. 4 and S8). Analysis of the TEY and FY data highlighted variations in chemical composition with depth, especially for electrochemically active species including Ni and Fe, impacted by the electrolyte formulation and inter-electrode cross-talk.

For both Ni and Fe, a higher intensity ratio of the high-to low-energy shoulders in the L3-edge spectra indicates an increased oxidation state, where reduction typically signifies electrolyte oxidation. For Ni, engagement of cross-talk results in a lower oxidation state for both control and 2 wt% DTD-containing electrolytes compared to samples without cross-talk, in both TEY (Fig. 4a) and FY (Fig. 4b) modes. This suggests that cross-talk promotes electrolyte oxidation irrespective of the CEI formed with or without DTD. In the presence of cross-talk (i.e., full-cell operation), both electrolytes exhibit similar Ni oxidation states across TEY and FY modes, highlighting the inherent anodic stability of the F4DEE solvent in preventing electrolyte oxidation from the top surface to subsurface. Notably, FY mode consistently shows higher oxidation states than TEY mode across all samples (Fig. 4c), indicating an oxidation state gradient that increases from the top surface to subsurface.

For Fe (Fig. 4d–f), observations largely mirror those for Ni, with a few key distinctions. First, in the presence of cross-talk, while subsurface Fe oxidation states are similar for both electrolytes in FY mode, the control electrolyte shows a slightly higher state at the top surface in TEY mode compared to the DTD-containing electrolyte. This indicates that the CEI formed with DTD may offer marginally reduced protection against electrolyte oxidation during storage when F4DEE is the solvent. This potentially shifts DTD's primary benefit toward a benign SEI formation on the HC anode for mitigating Na inventory loss. Second, with the addition of 2 wt% DTD, Fe oxidation states remain comparable with or without cross-talk in both TEY and FY modes, suggesting that the DTD-formed CEI effectively counters the oxidation-promoting effects of cross-talk, thereby contributing to overall mitigation of cathode-anode cross-talk. This may contribute to its mitigation of impedance growth as shown in Fig. 3c–e. For Mn, the oxidation state remained consistent at Mn^{4+} on the surface across all samples (Fig. S8).

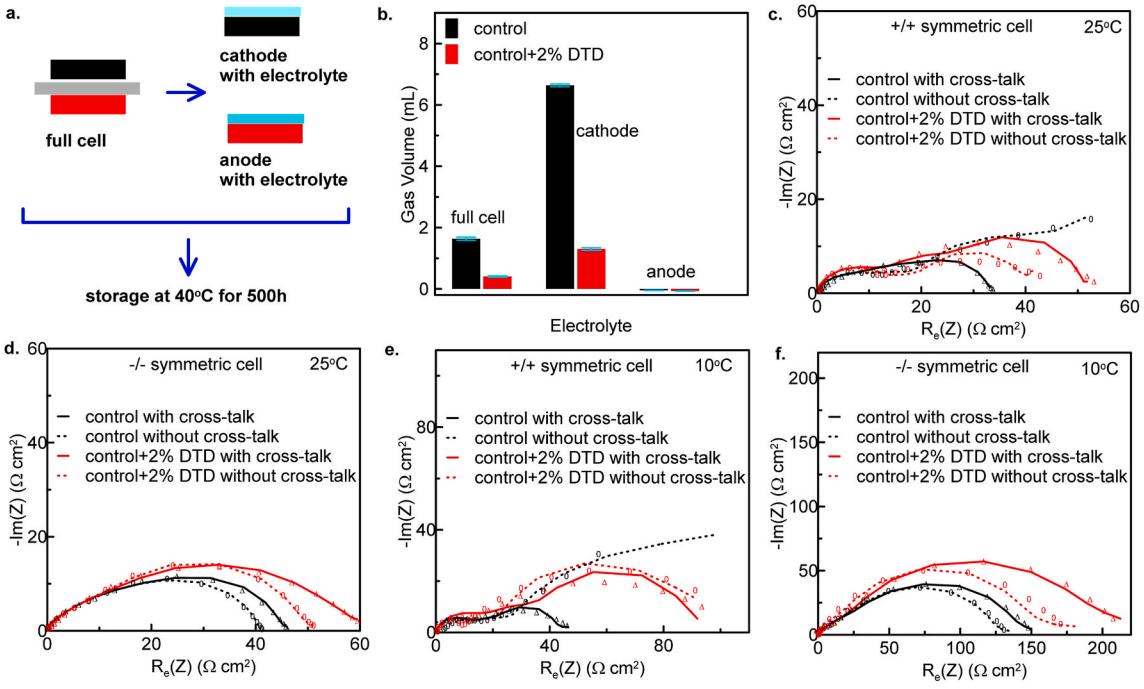

Fig. 3. Evaluation of the cathode-anode cross-talk. (a) A schematic of pouch bag method used for isolating cathode-anode cross-talk. (b) Gas volume of NCMFNZO/HC pouch cells, NCMFNZO or HC containing pouch bags with different electrolytes after 500h storage at 40 °C and 4.0V. (c–f) The Nyquist plot for (c, e) NCMFNZO/NCMFNZO and (d, f) HC/HC symmetric cells after 500h storage at 40 °C and 4.0V measured at (c, d) 25 °C and (e, f) 10 °C with equivalent circuit fitting. Experimental data are shown as solid line and fitted data are shown as triangle or circle symbol.

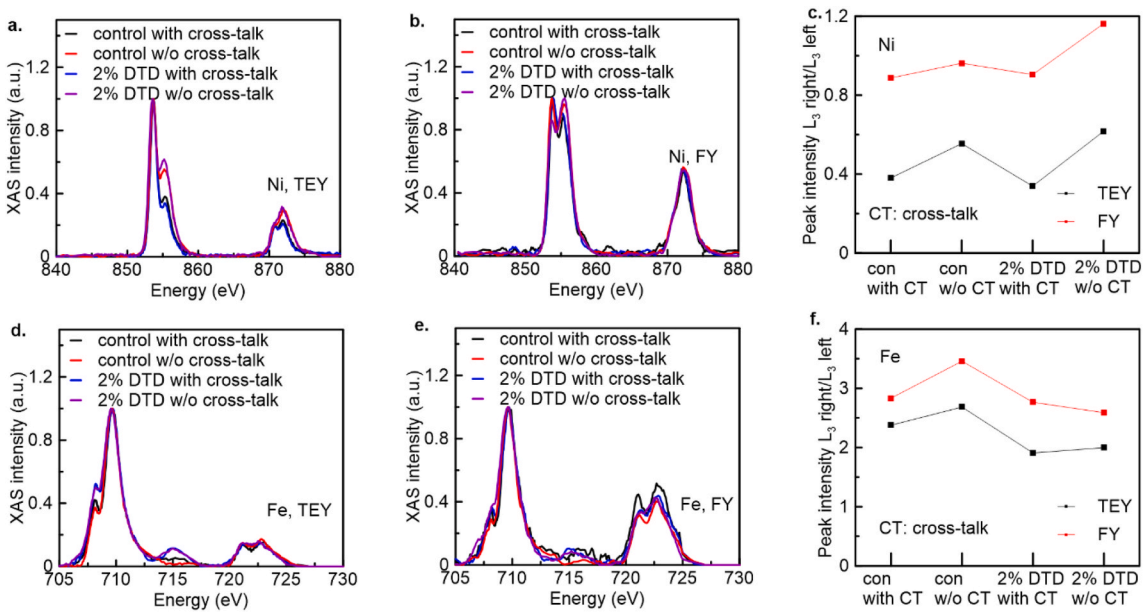

Fig. 4. Evaluation of CEI of NCMFNZO after 500h storage at 40 °C and 4.0V using soft XAS spectroscopy. (a–b) Ni L-edge for NCMFNZO cathode in (a) TEY and (b) FY mode. (c) The Ni L3-edge has two peaks, and the intensity ratio between the right peak and the left peak is plotted as a function of the labeled conditions. (d–e) Fe L-edge for NCMFNZO cathode in (d) TEY and (e) FY mode. (f) The Fe L3-edge has two peaks, and the intensity ratio between the right peak and the left peak is plotted as a function of the labeled conditions.

4. Conclusions

In summary, this study shows the synergistic effect of incorporating DTD as an electrolyte additive into a F4DEE-based electrolyte to enhance the performance of NCMFNZO/HC pouch cells. During formation, the DTD-containing electrolyte contributes to a stable CEI on the NCMFNZO cathode, as evidenced by suppressed transition metal reduction, while promoting NaF and sulfur-containing species in the SEI on the HC anode. NCMFNZO/HC pouch cells with DTD exhibit superior long-term cycling performance with a 4.0V upper cutoff limit, achieving capacity retention of ~88 % at 25 °C and ~82 % at 40 °C after 500 cycles at C/5, which is attributable to mitigated Na inventory loss and controlled polarization growth.

Isolation of cathode-anode cross-talk via pouch bag experiments highlights that F4DEE with DTD effectively suppresses gas generation at the cathode and impedance growth, particularly in the absence of cross-talk. These experiments highlight their role in affecting CEI evolution during 4.0 V, 40 °C, 500 h storage. Soft XAS analysis further elucidates the depth-dependent benefits of F4DEE solvent on mitigating electrolyte oxidation, showing maintained comparably high Ni and Fe oxidation states at the surface and subsurface with cross-talk. The addition of DTD slightly lowers the Fe oxidation state, indicating a modest reduction in the CEI's ability to prevent electrolyte oxidation during evolution; nonetheless, DTD preserves Fe oxidation with or without cross-talk, suggesting it promotes a CEI that mitigates cross-talk and correlates with controlled impedance growth. These findings show how DTD and F4DEE promotes robust interphases together, bridging fundamental insights into interphasial chemistry with practical advancements in SIB longevity.

This work introduces a novel class of fluorinated ether-based solvents that enable extended SIB operation when paired with DTD as an additive to tune the interphase. Further engineering efforts to fine-tune interphasial chemistry are essential to further enhance electrolyte oxidation prevention and mitigate sodium plating during long-term cycling. Such developments hold significant promise for realizing SIBs with exceptionally long lifetimes, ideally suited for grid energy storage applications.

CRediT authorship contribution statement

Rishivandhiga Jayakumar: Investigation, Formal analysis, Data curation. **Chanmonirath Michael Chak:** Formal analysis, Data curation. **Vadim Shipitsyn:** Formal analysis, Data curation. **Yuwei Zhu:** Formal analysis, Data curation. **Yunyuan Lu:** Formal analysis, Data curation. **Glenn Pastel:** Supervision, Investigation. **Zhiao Yu:** Supervision, Data curation. **Linqin Mu:** Formal analysis. **Wenhua Zuo:** Data curation. **Lin Ma:** Supervision, Project administration, Conceptualization.

Declaration of competing interest

The authors declare that they have no known competing financial interests or personal relationships that could have appeared to influence the work reported in this paper.

Acknowledgements

Dr. L.M. acknowledges the support by the US National Science Foundation Award No. 2301719. Dr. Mu acknowledges the support from the ASU startup funds. The authors also acknowledge the use of Beamline 8-2 with assistance from Dr. Dennis Nordlund at the Stanford Synchrotron Radiation Light source, SLAC National Accelerator Laboratory, which was supported by the U.S. Department of Energy, Office of Science, Office of Basic Energy Sciences under Contract no. DE-AC02-76SF00515. W.Z. thanks for the support from Office of Vehicle Technologies of the U.S. Department of Energy through LENS consortium (contract no. DE-AC02-06CH11357).

Appendix A. Supplementary data

Supplementary data to this article can be found online at https://doi.org/10.1016/j.jpowsour.2025.238753.

Data availability

Data will be made available on request.

References

[1] M.M. Hasan, R. Haque, M.I. Jahirul, M.G. Rasul, I.M.R. Fattah, N.M.S. Hassan, M. Mofijur, Advancing energy storage: the future trajectory of lithium-ion battery technologies, J. Energy Storage 120 (2025) 116511, https://doi.org/10.1016/j.est.2025.116511.

[2] M. Titirici, P. Johansson, M. Crespo Ribadeneyra, H. Au, A. Innocenti, S. Passerini, E. Petavratzi, P. Lusty, A.A. Tidblad, A.J. Naylor, R. Younesi, Y.A. Chart, J. Aspinall, M. Pasta, J. Orive, L.M. Babulal, M. Reynaud, K.G. Latham, T. Hosaka, S. Komaba, J. Bitenc, A. Ponrouch, H. Zhang, M. Armand, R. Kerr, P.C. Howlett, M. Forsyth, J. Brown, A. Grimaud, M. Vilkman, K.B. Dermenci, S. Mousavihashemi, M. Berecibar, J.E. Marshall, C.R. McElroy, E. Kendrick, T. Safdar, C. Huang, F. M. Zanotto, J.F. Troncoso, D.Z. Dominguez, M. Alabdali, U. Vijay, A.A. Franco, S. Pazhaniswamy, P.S. Grant, S. López Guzman, M. Fehse, M. Galceran, N. Antuñano, Roadmap for sustainable batteries, JPhys Energy 6 (4) (2024) 041502, https://doi.org/10.1088/2515-7655/ad6bc0.

[3] P. Phogat, S. Dey, M. Wan, Comprehensive review of sodium-ion batteries: principles, materials, performance, challenges, and future perspectives, Mater. Sci. Eng. B 312 (2025) 117870, https://doi.org/10.1016/j.mseb.2024.117870.

[4] Y. Gao, H. Zhang, J. Peng, L. Li, Y. Xiao, L. Li, Y. Liu, Y. Qiao, S. Chou, A 30-year overview of sodium-ion batteries, Carbon Energy 6 (6) (2024) e464, https://doi.org/10.1002/cey2.464.

[5] Y.S. Meng, V. Srinivasan, K. Xu, Designing better electrolytes, Science 378 (6624) (2022), https://doi.org/10.1126/science.abq3750.

[6] K. Xu, Electrolytes and interphases in Li-Ion batteries and beyond, Chem. Rev. 114 (23) (2014) 11503–11618, https://doi.org/10.1021/cr500003w.

[7] Z. Ye, H. Hijazi, W. Black, S. Azam, J.R. Dahn, M. Metzger, Impact of salts and linear carbonates on the performance of layered Oxide/Hard carbon sodium-ion pouch cells with Alkyl Carbonate electrolytes, J. Electrochem. Soc. 171 (4) (2024) 040522, https://doi.org/10.1149/1945-7111/ad3b73.

[8] W. Fan, W. Wang, Q. Xie, X. He, H. Li, J. Zhao, J. Nan, A sodium Bis (Fluorosulfonyl)Imide (NaFSI)-based multifunctional electrolyte stabilizes the performance of $NaNi_{1/3}Fe_{1/3}Mn_{1/3}O_2$/Hard carbon sodium-ion batteries, Chem. Eur J. 30 (43) (2024), https://doi.org/10.1002/chem.202401321.

[9] Y. Jin, P.M.L. Le, P. Gao, Y. Xu, B. Xiao, M.H. Engelhard, X. Cao, T.D. Vo, J. Hu, L. Zhong, B.E. Matthews, R. Yi, C. Wang, X. Li, J. Liu, J.-G. Zhang, Low-Solvation electrolytes for high-voltage sodium-ion batteries, Nat. Energy 7 (8) (2022) 718–725, https://doi.org/10.1038/s41560-022-01055-0.

[10] H. Hijazi, Z. Ye, E. Zsoldos, M. Obialor, W. Black, S. Azam, J.R. Dahn, M. Metzger, Can layered Oxide/Hard carbon sodium-ion pouch cells with simple electrolyte additives achieve better cycle life than LFP/Graphite cells? J. Electrochem. Soc. 171 (5) (2024) 050521 https://doi.org/10.1149/1945-7111/ad47da.

[11] H. Hijazi, Z. Ye, L. Zhang, J. Deshmukh, M.B. Johnson, J.R. Dahn, M. Metzger, Impact of sodium metal plating on cycling performance of layered Oxide/Hard carbon sodium-ion pouch cells with different voltage cut-offs, J. Electrochem. Soc. 170 (7) (2023) 070512, https://doi.org/10.1149/1945-7111/ace4fa.

[12] D.J. Xiong, R. Petibon, M. Nie, L. Ma, J. Xia, J.R. Dahn, Interactions between positive and negative electrodes in Li-Ion cells operated at high temperature and high voltage, J. Electrochem. Soc. 163 (3) (2016) A546–A551, https://doi.org/10.1149/2.0951603jes.

[13] R. Jayakumar, T.P. Pollard, O. Borodin, V. Shipitsyn, C. Chak, Michael, G. Pastel, A. Zheng, M. Johnson, F. Hasan, C.M. Bejger, M.A. Schroeder, S.G. Greenbaum, W. Zuo, L. Ma, Weakly solvating ester electrolyte for high voltage sodium-ion batteries, Nano Energy 128 (2024) 109969, https://doi.org/10.1016/j.nanoen.2024.109969.

[14] Y. Lin, Z. Yu, W. Yu, S.-L. Liao, E. Zhang, X. Guo, Z. Huang, Y. Chen, J. Qin, Y. Cui, Z. Bao, Impact of the fluorination degree of ether-based electrolyte solvents on Li-Metal battery performance, J. Mater. Chem. A 12 (5) (2024) 2986–2993, https://doi.org/10.1039/d3ta05535c.

[15] Z. Yu, P.E. Rudnicki, Z. Zhang, Z. Huang, H. Celik, S.T. Oyakhire, Y. Chen, X. Kong, S.C. Kim, X. Xiao, H. Wang, Y. Zheng, G.A. Kamat, M.S. Kim, S.F. Bent, J. Qin, Y. Cui, Z. Bao, Rational solvent molecule tuning for high-performance lithium metal battery electrolytes, Nat. Energy 7 (1) (2022) 94–106, https://doi.org/10.1038/s41560-021-00962-y.

[16] C.V. Amanchukwu, Z. Yu, X. Kong, J. Qin, Y. Cui, Z. Bao, A new class of ionically conducting fluorinated ether electrolytes with high electrochemical stability, J. Am. Chem. Soc. 142 (16) (2020) 7393–7403, https://doi.org/10.1021/jacs.9b11056.

[17] V. Shipitsyn, R. Jayakumar, W. Zuo, W. Yin, E. Huber, L. Ma, The impact of fluoroethylene carbonate additive on charged sodium ion Electrodes/Electrolyte reactivity studied using accelerating rate calorimetry, J. Electrochem. Soc. 170 (11) (2023) 110501, https://doi.org/10.1149/1945-7111/ad0665.

[18] C.P. Aiken, J. Xia, D.Y. Wang, D.A. Stevens, S. Trussler, J.R. Dahn, An Apparatus for the Study of in situ gas evolution in Li-Ion pouch cells, J. Electrochem. Soc. 161 (10) (2014) A1548–A1554, https://doi.org/10.1149/2.0151410jes.

[19] S. Tan, D. Kuai, Z. Yu, S. Perez-Beltran, M.M. Rahman, K. Xia, N. Wang, Y. Chen, X.-Q. Yang, J. Xiao, J. Liu, Y. Cui, Z. Bao, P.B. Balbuena, E. Hu, Evolution and interplay of lithium metal interphase components revealed by experimental and theoretical studies, J. Am. Chem. Soc. 146 (17) (2024) 11711–11718, https://doi.org/10.1021/jacs.3c14232.

[20] L. Madec, J. Xia, R. Petibon, K.J. Nelson, J.-P. Sun, I.G. Hill, J.R. Dahn, Effect of sulfate electrolyte additives on $LiNi_{1/3}Mn_{1/3}Co_{1/3}O_2$/Graphite pouch cell lifetime: correlation between XPS surface studies and electrochemical Test results, J. Phys. Chem. C 118 (51) (2014) 29608–29622, https://doi.org/10.1021/jp509731y.

[21] J. Fu, X. Ji, J. Chen, L. Chen, X. Fan, D. Mu, C. Wang, Lithium nitrate regulated sulfone electrolytes for lithium metal batteries, Angew. Chem. Int. Ed. 59 (49) (2020) 22194–22201, https://doi.org/10.1002/anie.202009575.

[22] L. Mu, X. Feng, R. Kou, Y. Zhang, H. Guo, C. Tian, C. Sun, X. Du, D. Nordlund, H. L. Xin, F. Lin, Deciphering the cathode–electrolyte interfacial chemistry in sodium layered cathode materials, Adv. Energy Mater. 8 (34) (2018), https://doi.org/10.1002/aenm.201801975.

[23] L. Mu, D. Hou, E.E. Foley, M. Dai, J. Zhang, Z. Jiang, M.M. Rahman, Y. Fu, L. Ma, E. Hu, S. Sainio, D. Nordlund, J. Liu, J.-M. Hu, Y. Liu, R.J. Clément, F. Lin, Revealing the chemical and structural complexity of electrochemical ion exchange in layered oxide materials, J. Am. Chem. Soc. 146 (39) (2024) 26916–26925, https://doi.org/10.1021/jacs.4c08089.